

[Nature, in review]

Spin correlations of the electron-doped high transition-temperature superconductor $\text{Nd}_{2-x}\text{Ce}_x\text{CuO}_4$

E.M. Motoyama¹, G. Yu¹, I.M. Vishik¹, O.P. Vajk², P.K. Mang³ & M. Greven^{3,4}

¹*Department of Physics, Stanford University, Stanford, California 94305, USA*

²*NIST Center for Neutron Research, National Institute of Standards and Technology, Gaithersburg, Maryland 20899, USA*

³*Department of Applied Physics, Stanford University, Stanford, California 94305, USA*

⁴*Stanford Synchrotron Radiation Laboratory, Stanford, California 94309, USA*

High transition-temperature (T_c) superconductivity develops near antiferromagnetic phases, and it is possible that magnetic excitations contribute to the superconducting pairing mechanism. In order to assess the role of antiferromagnetism, it is essential to understand the doping and temperature dependence of the two-dimensional antiferromagnetic spin correlations. Here we report inelastic magnetic neutron scattering measurements on the electron-doped superconductor $\text{Nd}_{2-x}\text{Ce}_x\text{CuO}_4$. The data demonstrate that long-range antiferromagnetism and superconductivity do not co-exist. Instead, there exists a magnetic quantum critical point where superconductivity first appears, consistent with an exotic quantum phase transition between the two phases.¹ Photoemission^{2,3}, optical spectroscopy^{4,5}, and charge transport⁵ experiments have revealed pronounced charge anomalies below a characteristic ‘pseudogap’ temperature T_{χ} associated with the opening of a partial gap of the electronic

states along the Fermi surface. We demonstrate that the pseudogap in the electron-doped materials arises from a build-up of spin correlations, in agreement with recent theoretical proposals^{6,7}.

Since the charge carriers in the copper-oxygen sheets can be either electrons or holes, the high- T_c phase diagram is divided into two halves. Upon doping with holes, the commensurate AF phase quickly disappears⁸, and the low-energy magnetic response becomes incommensurate with the crystal lattice as the system evolves into a superconductor^{9,10}. In the comparatively less-studied electron-doped copper oxides, the commensurate AF phase extends much farther and appears to overlap with the superconducting (SC) phase¹¹⁻¹⁴. In fact, as-grown samples exhibit AF order throughout the accessible doping range, and an oxygen reduction treatment is required in order to induce superconductivity¹⁵. In oxygen-reduced samples of the archetypical compound $\text{Nd}_{2-x}\text{Ce}_x\text{CuO}_4$ (NCCO), evidence for AF order has been found up to $x = 0.17$ ^{13,14}, while the system shows bulk superconductivity above $x_{\text{SC}} = 0.13$ ¹². The highest transition temperature of $T_c = 25\text{K}$ is achieved for $x = 0.15$, which is referred to as optimal doping. The pseudogap temperature (and the associated gap energy) extrapolates to zero at $x = 0.17$ in the SC doping regime (See Fig. 1)^{4,5}. Both the AF order and the anomalous charge behaviour appear to vanish at approximately the same doping concentration, and it has been suggested that the electron-doped compounds undergo a quantum phase transition related to the disappearance of AF order at this point of the phase diagram^{4,16}.

Neutron scattering is a powerful probe of magnetic excitations, and for the study of low-

dimensional systems with strong quantum fluctuations, it requires the use of large single crystals. While such measurements have provided essential information about the spin dynamics in hole-doped compounds^{8,17,18}, they have only recently become possible in the electron-doped superconductors^{19,20}. In this study, we take advantage of the two-dimensional (2D) nature of the system and use appropriate spectrometer configurations to integrate over a large window in energy, from $k_B T$ up to the incident neutron energy (E_i), significantly improving signal rates. If the energy window encompasses the characteristic dynamic energy scale of the system, it is possible to measure the 2D instantaneous spin-spin correlation length near the transition to long-range magnetic order. This so-called ‘two-axis’ technique was used with great success in studies of undoped and hole-doped La_2CuO_4 ^{8,21}. Experiments on as-grown, non-SC NCCO demonstrated that the 2D spin correlation length observed above the Néel temperature is exponentially dependent on inverse temperature,

$$(x;T) = A(x) \exp(2\zeta_s(x) = T); \quad (1)$$

for Ce concentrations ranging from zero up to the solubility limit of $x = 0.18$. This behaviour indicates the existence of an underlying ground state with long-range 2D AF order. Due to weak spin-space anisotropies and three-dimensional couplings, NCCO exhibits three-dimensional AF order at a non-zero Néel temperature, as observed in the elastic scattering channel^{11,14}. The spin stiffness $\zeta_s(x)$ decreases monotonically with increasing electron concentration, with $\zeta_s(0.18) = \zeta_s(0) - 25\%$ ¹⁴, and the doping dependence of $\zeta_s(x)$ and of the amplitude $A(x)$ is remarkably close to that for the randomly-diluted spin-1/2 square-lattice Heisenberg antiferromagnet $\text{La}_2\text{Cu}_{1-x}(\text{Zn},\text{Mg})_x\text{O}_4$ ²².

We have carried out two-axis measurements in eight oxygen-reduced NCCO crystals in the

Ce concentration range $0.038 \leq x \leq 0.154$. Representative scans for the instantaneous structure factor $S(Q)$ are shown in Fig. 2. The data are fit to a 2D Lorentzian, $S(Q_{2D}) = S(0) = (1 + Q_{2D}^2)^{-2}$, convoluted with the calculated instrumental resolution, where Q_{2D} is the distance in momentum space from the 2D AF zone center.

Figure 3 shows the temperature and doping dependence of the correlation length. The non-SC samples ($x \leq 0.129$) follow equation (1), consistent with bulk AF order in the ground state. While this behaviour is qualitatively the same as that for as-grown NCCO¹⁴, the spin stiffness decreases much more rapidly with doping. The SC sample with $x = 0.134$ is fit to equation (1) with a small value of the spin stiffness ζ_s , but it is equally well described by the simple power law $\zeta \propto T^{-\zeta_s}$ with exponent $\zeta_s = 1.0(5)$. The power-law behaviour, indicated by the dashed curve in Figure 3, would imply that ζ_s is already zero and that the system is quantum critical at this Ce concentration. Figure 4a demonstrates that ζ_s approaches zero at $x_{AF} = 0.134(4)$ in an approximately linear fashion. In a fundamental departure from the above behaviour, we find that in the SC samples with $x \geq 0.145$, ζ_s remains finite down to the lowest temperatures. This demonstrates that, contrary to previous belief^{4,12,16}, the ground state does not exhibit genuine magnetic order. The low-temperature correlation length ζ_0 for these samples is found to increase as x_{AF} is approached from above, as shown in Fig. 4a.

Previous elastic neutron measurements^{11,12,14} indicated that oxygen-reduced NCCO exhibits AF order up to $x = 0.17$. Such measurements in our crystals indeed reveal Néel order. However, our inelastic neutron scattering results demonstrate that the ground state of SC samples only

exhibits short-range spin correlations. Moreover, inelastic neutron scattering experiments clearly revealed a SC magnetic gap, despite the presence of AF Bragg peaks in the elastic response^{19,20}. We conclude that the AF phase boundary in fact terminates at $x_{AF} = 0.134(4)$, and that magnetic Bragg peaks observed at higher Ce concentrations originate from regions of the samples which were not fully oxygen-annealed. While a relatively small volume fraction of such remnants of the AF as-grown state can give rise to significant Bragg scattering, our inelastic measurements are fortunately insensitive to their presence. This conclusion is consistent with the observation that the Néel transition is very broad in SC samples (see Fig. 4b), and also with muon spin resonance results¹², which show a significant decrease of the AF volume fraction near $x = 0.14$. We note that the spurious elastic signal from the remnant AF regions should not be confused with the spurious elastic signal in a magnetic field²³ due to the paramagnetic decomposition product $(Nd,Ce)_2O_3$.

We now estimate the underlying bulk Néel temperature in the hypothetical absence of as-grown remnants. For as-grown NCCO¹⁴ and $La_2Cu_{1-x}(Zn,Mg)_xO_4$ ²² it was found that, to a very good approximation, the Néel temperature $T_N(x)$ is a contour of constant 2D correlation length with $=a = 200-400$ and 100, respectively. Following the observations for as-grown NCCO, we plot the extrapolated contour of $=a = 400$ as a dashed curve in Fig. 1. This contour coincides with the measured T_N at $x = 0.038$, but it lies systematically lower at higher Ce concentrations, approaching $T_N = 0$ at $x_{AF} = 0.134$.

The decrease to zero of the spin stiffness at $x_{AF} = 0.134$ and the finite values of ω_0 for $x > x_{AF}$ indicates a fundamental change in the nature of the magnetic ground state. While the

contribution of the AF remnants may lead to a slight over-estimate of the spin correlations, and consequently of χ_s and χ_0 , we emphasize that the qualitative change in behaviour is a robust result. The NCCO phase diagram resembles those of other unconventional superconductors, such as the heavy-fermion compound CeRhIn₅, where the AF and SC phases are believed to be separated by a first-order boundary²⁴. While we cannot rule out a genuine underlying coexistence between AF and SC order, such a coexistence would be confined to a rather narrow doping range. However, the behaviour of $\chi_s(x)$, which decreases continuously by more than an order of magnitude with doping, together with the cross-over to power-law behaviour of $\chi(x;T)$ near $x = 0.134$, points to another scenario: a second-order quantum phase transition between the AF and SC phases. This quantum phase transition would be described by a dynamic critical exponent of $z = 1 = \zeta_T = 1.0(5)$, which differs from the value $z = 2$ predicted for a transition from the AF to a non-SC paramagnet⁶. If hyperscaling holds, the spin stiffness for a 2D system is expected to decrease as $\chi_s \propto (x_{AF} - x)^{\zeta_0 z}$, where ζ_0 is the exponent describing the divergence of χ_0 as x_{AF} is approached from above. From the approximately linear behaviour of the spin stiffness, we therefore have $\zeta_0 = 1$. We cannot independently determine ζ_0 , since we do not have sufficient information for $\chi_0(x)$. It is also possible that the system lies above the upper critical dimension, in which case mean-field behaviour with $\chi_s \propto (x_{AF} - x)^{2 - \zeta_M F}$ is expected. Since $\zeta_M F = 1/2$, this is consistent with the observed behaviour.

Our results for $\chi(x;T)$ have important consequences for the relationship between AF correlations and the pseudogap physics in the electron-doped copper oxides, which appears to be different from the hole-doped materials⁵⁻⁷. The pseudogap has been discerned up to $x = 0.15$ in both pho-

to emission on NCCO crystals² and optical spectroscopy on $\text{Pr}_{2-x}\text{Ce}_x\text{CuO}_4$ films⁴. We find that the spin correlation length changes smoothly across T and, in Fig. 4c, we plot $\langle x; T \rangle$.

Remarkably, up to optimal doping, this quantity follows the simple relationship

$$\frac{1}{a} = \frac{C}{x_c - x}; \quad (2)$$

with $C = 0.96(12)$ and $x_c = 0.171(4)$. One interpretation of the pseudogap is that it signifies an increase of spin scattering of the electrons as the AF correlations exceed the carrier mean free path⁵ (λ) or the single-particle thermal de Broglie wavelength⁶ ($\lambda_{\text{th}} = h\nu_F = k_B T$) upon cooling. Boltzmann transport theory, which might be expected to qualitatively hold if $\lambda > a$ and $T > T_c$, applied to DC resistivity data for NCCO yields $\lambda(T) = 2.4a$ and $\lambda = 25a$ for $x = 0.125$ and $x = 0.15$, respectively⁵. This trend is qualitatively consistent with our results up to $x = 0.145$ seen in Fig. 4c. However, given the approximately linear relationship $T_c / \langle x; x \rangle$ (Fig. 1), the thermal de Broglie wavelength at T_c exhibits the same *quantitative* doping dependence as equation (2). Using the value $v_F = 2.2 \times 10^7 \text{ cm/s}$ for the bare Fermi velocity⁶, we find that $\lambda_{\text{th}} = 2.6(2) \text{ } \mu\text{m}$. We conclude that T_c is a cross-over temperature below which the spin correlations become longer than the thermal de Broglie wavelength, in agreement with theoretical work⁶. The pseudogap phenomenon in the electron-doped copper oxides therefore results from 2D AF spin correlations, and does not appear to be a direct precursor to superconductivity. We note that the fact that $\lambda_{\text{th}} / \langle x; x \rangle$ is obeyed so well confirms that the contributions from the remnant AF regions to our measured $\langle x; T \rangle$ are negligible.

Equation (2) would suggest that λ diverges at $x_c = x$. However, as seen from Fig. 4c, this relation breaks down near optimal doping, presumably due to the emergence of a new length

scale that limits the development of spin correlations. Interestingly, at optimal doping, $\text{Nd}_{2-x}\text{Ce}_x\text{CuO}_4$ ⁰ is comparable to the SC coherence length²⁵ $\lambda_{\text{SC}} = 58 \text{ \AA} \approx 15 \text{ \AA}$. The spin correlations near optimal doping are still relatively large, consistent with suggestions based on Raman scattering²⁶ and photoemission²⁷ that the $d_{x^2-y^2}$ SC order parameter is non-monotonic due to AF fluctuations.

By avoiding spurious scattering that significantly contaminates the elastic response, we have established from measurements of the 2D spin correlations that genuine coexistence of antiferromagnetism and superconductivity is essentially absent in $\text{Nd}_{2-x}\text{Ce}_x\text{CuO}_4$. The new experimental results contain important implications for theories of high- T_c superconductivity. On symmetry grounds, a second-order quantum phase transition between these two types of order would seem unlikely and exotic. One possible scenario is that an underlying first-order transition is rendered second-order due to microscopic disorder²⁸. Such disorder is found in most high- T_c superconductors²⁹ and, in the present case, it might be the randomness associated with the Nd-Ce substitution. Alternatively, the phase transition may be an example of ‘deconfined’ quantum criticality¹, a new paradigm for quantum phase transitions.

1. Senthil, T., Vishwanath, A., Balents, L., Sachdev, S. & Fisher, M. P. A. Deconfined quantum critical points. *Science* **303**, 1490–1494 (2004).
2. Armitage, N. P. *et al.* Doping dependence of an n-type cuprate superconductor investigated by angle-resolved photoemission spectroscopy. *Phys. Rev. Lett.* **88**, 257001 (2002).
3. Matsui, H. *et al.* Angle-resolved photoemission spectroscopy of the antiferromagnetic superconductor $\text{Nd}_{1.87}\text{Ce}_{0.13}\text{CuO}_4$: Anisotropic spin-correlation gap, pseudogap, and the induced

quasiparticle mass enhancement. *Phys. Rev. Lett.* **94**, 047005 (2005).

4. Zimmers, A. *et al.* Infrared properties of electron-doped cuprates: Tracking normal-state gaps and quantum critical behavior in $\text{Pr}_{2-x}\text{Ce}_x\text{CuO}_4$. *Europhys. Lett.* **70**, 225–231 (2005).
5. Onose, Y., Taguchi, Y., Ishizaka, K. & Tokura, Y. Charge dynamics in underdoped $\text{Nd}_{2-x}\text{Ce}_x\text{CuO}_4$: Pseudogap and related phenomena. *Phys. Rev. B* **69**, 024504 (2004).
6. Kyung, B., Hankevych, V., Daré, A.-M. & Tremblay, A.-M. S. Pseudogap and spin fluctuations in the normal state of the electron-doped cuprates. *Phys. Rev. Lett.* **93**, 147004 (2004).
7. Markiewicz, R. S. Mode-coupling model of Mott gap collapse in the cuprates: Natural phase boundary for quantum critical points. *Phys. Rev. B* **70**, 174518 (2004).
8. Keimer, B. *et al.* Magnetic excitations in pure, lightly doped, and weakly metallic La_2CuO_4 . *Phys. Rev. B* **46**, 14034–14053 (1992).
9. Yamada, K. *et al.* Doping dependence of the spatially modulated dynamical spin correlations and the superconducting-transition temperature in $\text{La}_{2-x}\text{Sr}_x\text{CuO}_4$. *Phys. Rev. B* **57**, 6165–6172 (1998).
10. Matsuda, M. *et al.* Static and dynamic spin correlations in the spin-glass phase of slightly doped $\text{La}_{2-x}\text{Sr}_x\text{CuO}_4$. *Phys. Rev. B* **62**, 9148–9154 (2000).
11. Matsuda, M. *et al.* Magnetic order, spin correlations, and superconductivity in single-crystal $\text{Nd}_{2-x}\text{Ce}_x\text{CuO}_{4+}$. *Phys. Rev. B* **45**, 12548–12554 (1992).

12. Uefuji, T. *et al.* Coexistence of antiferromagnetic ordering and high- T_c superconductivity in electron-doped superconductor $\text{Nd}_{2-x}\text{Ce}_x\text{CuO}_4$. *Physica C* **357-360**, 208–211 (2001).

13. Uefuji, T., Kurahashi, K., Fujita, M., Matsuda, M. & Yamada, K. Electron-doping effect on magnetic order and superconductivity in $\text{Nd}_{2-x}\text{Ce}_x\text{CuO}_4$ single crystals. *Physica C* **378-381**, 273–277 (2002).

14. Mang, P. K., Vajk, O. P., Arvanitaki, A., Lynn, J. W. & Greven, M. Spin correlations and magnetic order in nonsuperconducting $\text{Nd}_{2-x}\text{Ce}_x\text{CuO}_4$. *Phys. Rev. Lett.* **93**, 027002 (2004).

15. Tokura, Y., Takagi, H. & Uchida, S. A superconducting copper oxide compound with electrons as the charge carriers. *Nature* **337**, 345–347 (1989).

16. Dagan, Y. *et al.* Origin of the anomalous low temperature upturn in the resistivity of the electron-doped cuprate superconductors. *Phys. Rev. Lett.* **94**, 057005 (2005).

17. Rossat-Mignod, J. *et al.* Neutron scattering study of the $\text{YBa}_2\text{Cu}_3\text{O}_{6+x}$ system. *Physica C* **185-189**, 86–92 (1991).

18. Yamada, K. *et al.* Direct observation of a magnetic gap in superconducting $\text{La}_{1.85}\text{Sr}_{0.15}\text{CuO}_4$ ($T_c = 37.3\text{ K}$). *Phys. Rev. Lett.* **75**, 1626–1629 (1995).

19. Yamada, K. *et al.* Commensurate spin dynamics in the superconducting state of an electron-doped cuprate superconductor. *Phys. Rev. Lett.* **90**, 137004 (2003).

20. Motoyama, E. M. *et al.* Magnetic field effect on the superconducting magnetic gap of $\text{Nd}_{1.85}\text{Ce}_{0.15}\text{CuO}_4$. *Phys. Rev. Lett.* **96**, 137002 (2006).

21. Birgeneau, R. J. *et al.* Instantaneous spin correlations in La_2CuO_4 . *Phys. Rev. B* **59**, 13788–13794 (1999).

22. Vajk, O. P., Mang, P. K., Greven, M., Gehring, P. M. & Lynn, J. W. Quantum impurities in the two-dimensional spin one-half Heisenberg antiferromagnet. *Science* **295**, 1691–1695 (2002).

23. Mang, P. K. *et al.* Phase decomposition and chemical inhomogeneity in $\text{Nd}_{2-x}\text{Ce}_x\text{CuO}_4$. *Phys. Rev. B* **70**, 094507 (2004).

24. Park, T. *et al.* Hidden magnetism and quantum criticality in the heavy fermion superconductor CeRhIn_5 . *Nature* **440**, 65–68 (2006).

25. Wang, Y. *et al.* Dependence of upper critical field and pairing strength on doping in cuprates. *Science* **299**, 86–89 (2003).

26. Blumberg, G. *et al.* Nonmonotonic $d_{x^2-y^2}$ superconducting order parameter in $\text{Nd}_{2-x}\text{Ce}_x\text{CuO}_4$. *Phys. Rev. Lett.* **88**, 107002 (2002).

27. Matsui, H. *et al.* Direct observation of a nonmonotonic $d_{x^2-y^2}$ -wave superconducting gap in the electron-doped high- T_c superconductor $\text{Pr}_{0.89}\text{LaCe}_{0.11}\text{CuO}_4$. *Phys. Rev. Lett.* **95**, 017003 (2005).

28. Aizenman, M. & Wehr, J. Rounding effects of quenched randomness on first-order phase transitions. *Commun. Math. Phys.* **130**, 489–528 (1990).

29. Eisaki, H. *et al.* Effect of chemical inhomogeneity in bismuth-based copper oxide superconductors. *Phys. Rev. B* **69**, 064512 (2004).

Acknowledgements The authors thank N. Bontemps, S. Chakravarty, S.A. Kivelson, R.S. Markiewicz and A.-M.S. Tremblay for discussions. The work at Stanford University was supported by grants from the Department of Energy and the National Science Foundation. E.M. acknowledges support through the NSF Graduate Fellowship program.

Author Information Reprints and permissions information is available at npg.nature.com/reprintsandpermissions. The authors declare no competing financial interests. Correspondence and requests for materials should be addressed to M.G. (greven@stanford.edu).

Figure 1 The temperature-doping phase diagram for oxygen-reduced $\text{Nd}_{2-x}\text{Ce}_x\text{CuO}_4$.

The red and blue hashed areas indicate long-range AF order and superconductivity, respectively. The black circle at zero temperature indicates the approximate location of a magnetic quantum phase transition. The instantaneous 2D spin correlation length $\langle x; T \rangle$ in the CuO_2 sheets was measured at the doping levels and over the temperature ranges indicated by the vertical bars. The colour map shows interpolated and extrapolated from the measured values. The Néel temperature T_N was determined from magnetic Bragg scattering measurements and is shown as the dotted curve, while the dashed curve is the extrapolated contour of $\langle x; T \rangle = 400$. The measurements of T_N , especially at higher doping levels, are contaminated by remnants of the as-grown state of NCCO, so that the true AF phase extends only to $x_{AF} = 0.13$, close to where superconductivity first appears. This is established from the fact that $\langle x; T \rangle$ diverges exponentially upon cooling for non-superconducting compositions at lower electron concentrations, while it remains finite in superconducting samples. The small remaining overlap indicated in the Figure may be caused by the Ce and oxygen inhomogeneities. The grey and white circles indicate optical conductivity measurements of $\langle x; T \rangle$ on NCCO crystals⁵ and $\text{Pr}_{2-x}\text{Ce}_x\text{CuO}_4$ thin films⁴, respectively. The dot-dashed curve is a guide to the eye.

Figure 2 Representative two-axis $\langle H; H \rangle$ scans for $\text{Nd}_{2-x}\text{Ce}_x\text{CuO}_4$ centred at the 2D AF zone center $(\frac{1}{2}; \frac{1}{2})$. Scans are fit (solid curves) to a 2D Lorentzian convoluted with the calculated instrumental resolution (dashed curves). Shown are data at **a**, $T = 250\text{K}$ $\langle x; T \rangle = T_N$ and **b**, $T = 400\text{K}$ for $x = 0.038$; **c**, $T = 300\text{K}$ for $x = 0.106$; **d**, $T = 35\text{K}$ and **e**, $T = 200\text{K}$

for $x = 0.145$; and f , $T = 1.8\text{ K}$ for $x = 0.154$. Wavevectors are represented as $(H; K; L)$ in reciprocal lattice units (r.l.u.), where $Q = (2H/a; 2K/a; 2L/c)$ is the momentum transfer, and a and c are the lattice constants of the tetragonal system (space group $I4/mmm$). For $x = 0.038$, room-temperature lattice constants are $a = 3.93\text{ \AA}$ and $c = 12.09\text{ \AA}$. The measurements were performed on the BT2 and BT9 triple-axis spectrometers at the NIST Center for Neutron Research. The incident neutron energy was $E_i = 14.7\text{ meV}$. In previous experiments on La_2CuO_4 ²¹, $\text{La}_{2-x}(\text{Zn},\text{Mg})_x\text{O}_4$ ²² and as-grown NCCO¹⁴, this energy proved to be sufficiently large in the temperature region $T_N < T < 2T_N$ to reliably extract the instantaneous structure factor $S(Q)$. The collimations were: **a**, **b**, 40° - 23° -sample- 20° ; **c**, 60° - 40° -sample- 40° ; **d**, 40° - 47° -sample- 10° ; **e**, 40° - 47° -sample- 20° ; and **f**, 40° - 47° -sample- 40° . The NCCO crystals were grown in 4 atm of oxygen using the travelling-solvent floating-zone technique, and subsequently annealed for 10 hours at $970\text{ }^\circ\text{C}$ in argon, followed by 20 hours at $500\text{ }^\circ\text{C}$ in oxygen. The sample masses range from 1 g to 5 g . The oxygen reduction treatment, required for superconductivity to appear, is a non-equilibrium process resulting in unavoidable oxygen inhomogeneities. Ce concentrations x were determined from inductively coupled plasma (ICP) spectroscopy, with typical gradients of $x = 0.005$ along the growth direction. Superconductivity was observed from magnetic susceptibility measurements for $x = 0.134$.

Figure 3 The instantaneous spin-spin correlation length ζ , plotted in units of the planar lattice constant a , as a function of temperature at eight Ce concentrations x . The data for $x = 0.134$ are fit to equation (1). The spin stiffness may already be zero for $x = 0.134$,

since a fit to a simple power law $\propto 1/T$ describes the data equally well (dashed curve); power-law behaviour is expected at a quantum critical point. For $x = 0.145$ and higher, \propto does not diverge, but instead remains finite at low temperatures, demonstrating the absence of genuine AF order. The curves drawn for these latter data are guides to the eye. Superconductivity was observed for $x = 0.134$.

Figure 4 Spin stiffness, spin correlations at low-temperature, apparent Néel temperature, and spin correlations along T . **a**, Doping dependence of the spin stiffness $\propto s$ (plotted as $2\propto s=J$, where $J = 125\text{ meV}$ is the AF superexchange for the undoped Mott insulator Nd_2CuO_4 ^{11,14}) and of the low-temperature spin correlation length $\propto 0$. Dashed curves are guides to the eye. The spin stiffness decreases smoothly with doping and reaches zero in an approximately linear fashion around $x_{\text{AF}} = 0.134$. The ground state for $x < x_{\text{AF}}$ has long-range AF order, whereas long-range order is absent for $x > x_{\text{AF}}$, as seen from the finite values of $\propto 0$. The doping dependence of $\propto 0$ indicates a divergence as the critical point is approached from the right. **b**, Apparent Néel temperature T_N , as determined from elastic scattering, as a function of doping. The temperature dependence of the measured order parameter (not shown) was modelled using a Gaussian distribution of T_N , and the vertical bars indicate the FWHM of this distribution. The width increases with doping, consistent with the evidence that genuine magnetic order is absent for $x > 0.134$. Measurements were not performed on all samples; previous data¹⁴ are indicated by open symbols. The dotted and dashed curves are the same as in Fig. 1. **c**, The spin correlation length \propto measured at or extrapolated to the pseudogap temperature T . Below optimal

doping ($x < 0.15$), λ is given by the single-particle thermal de Broglie wavelength and increases as $\lambda \propto 1/(x - x_0)$ (fitted curve). However, this relationship breaks down near optimal doping, where λ is found not to exceed the SC coherence length.

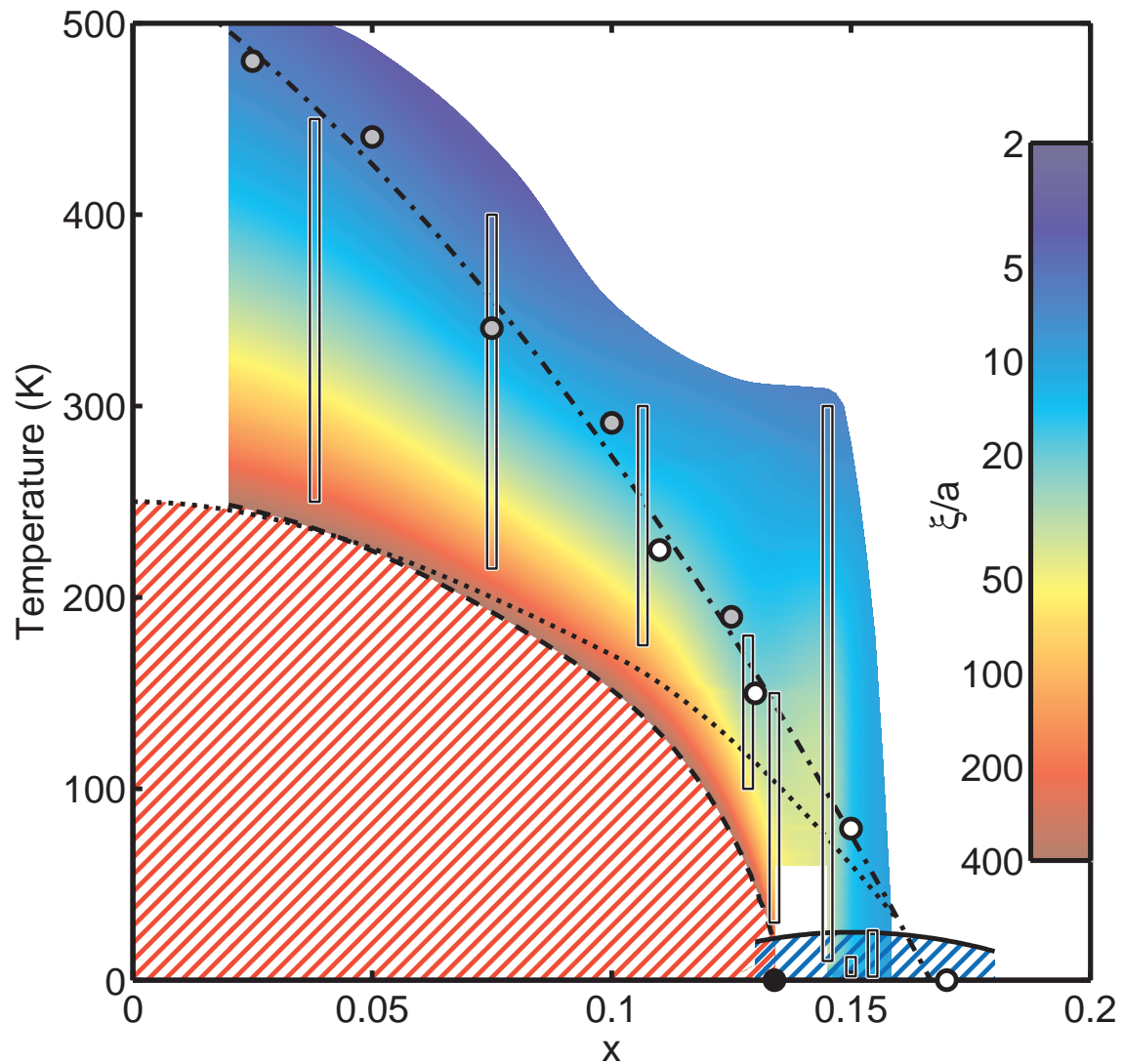


Figure 1

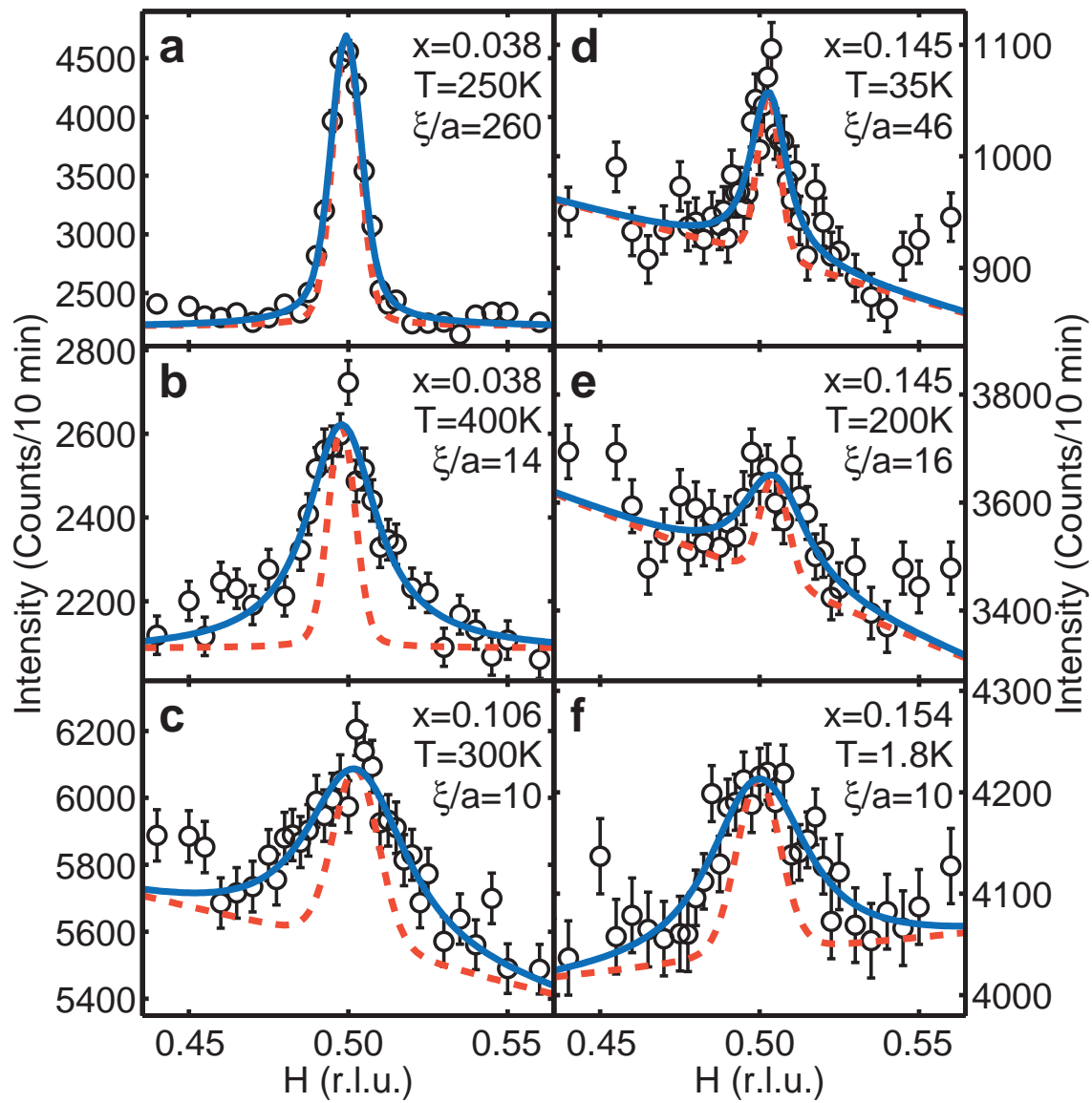


Figure 2

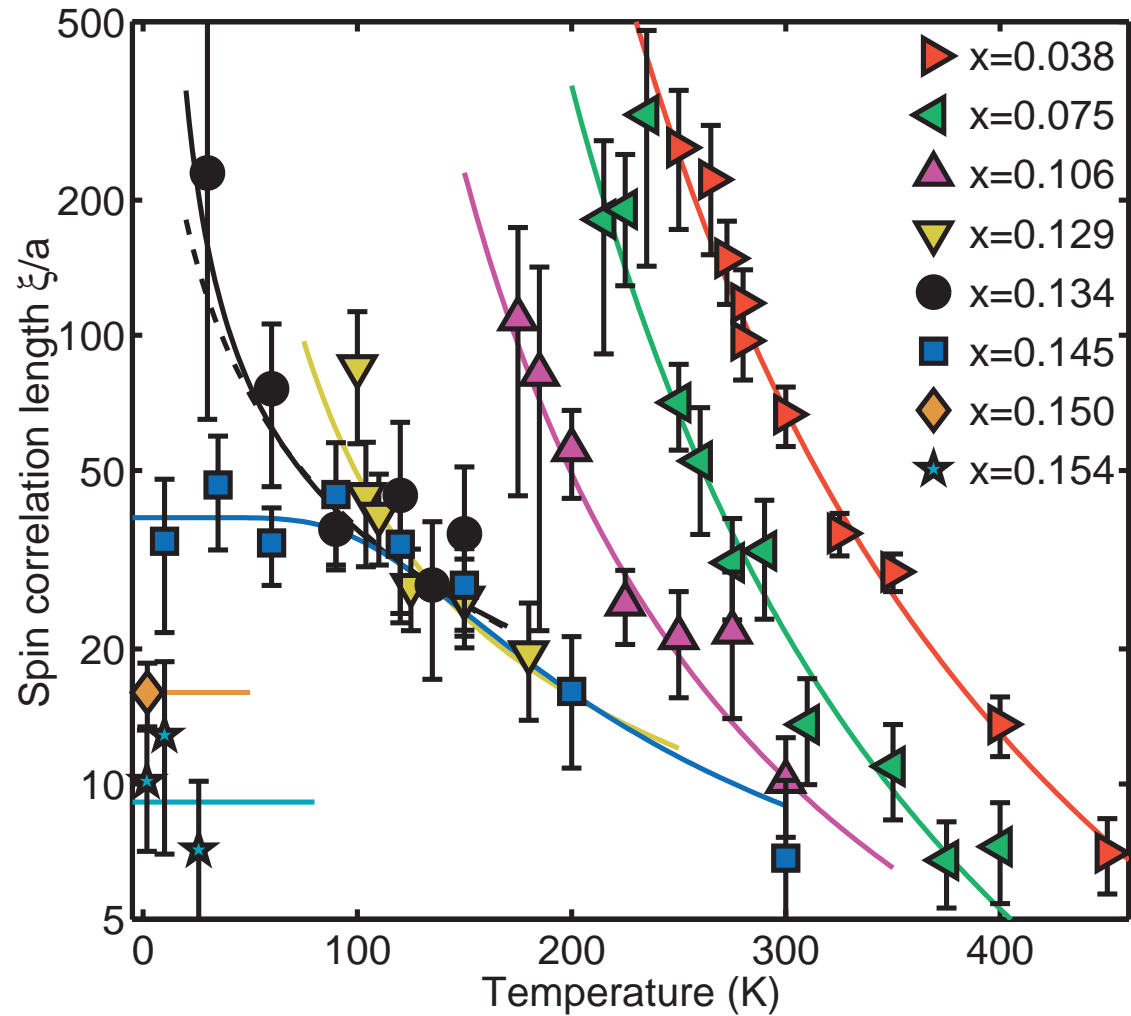


Figure 3

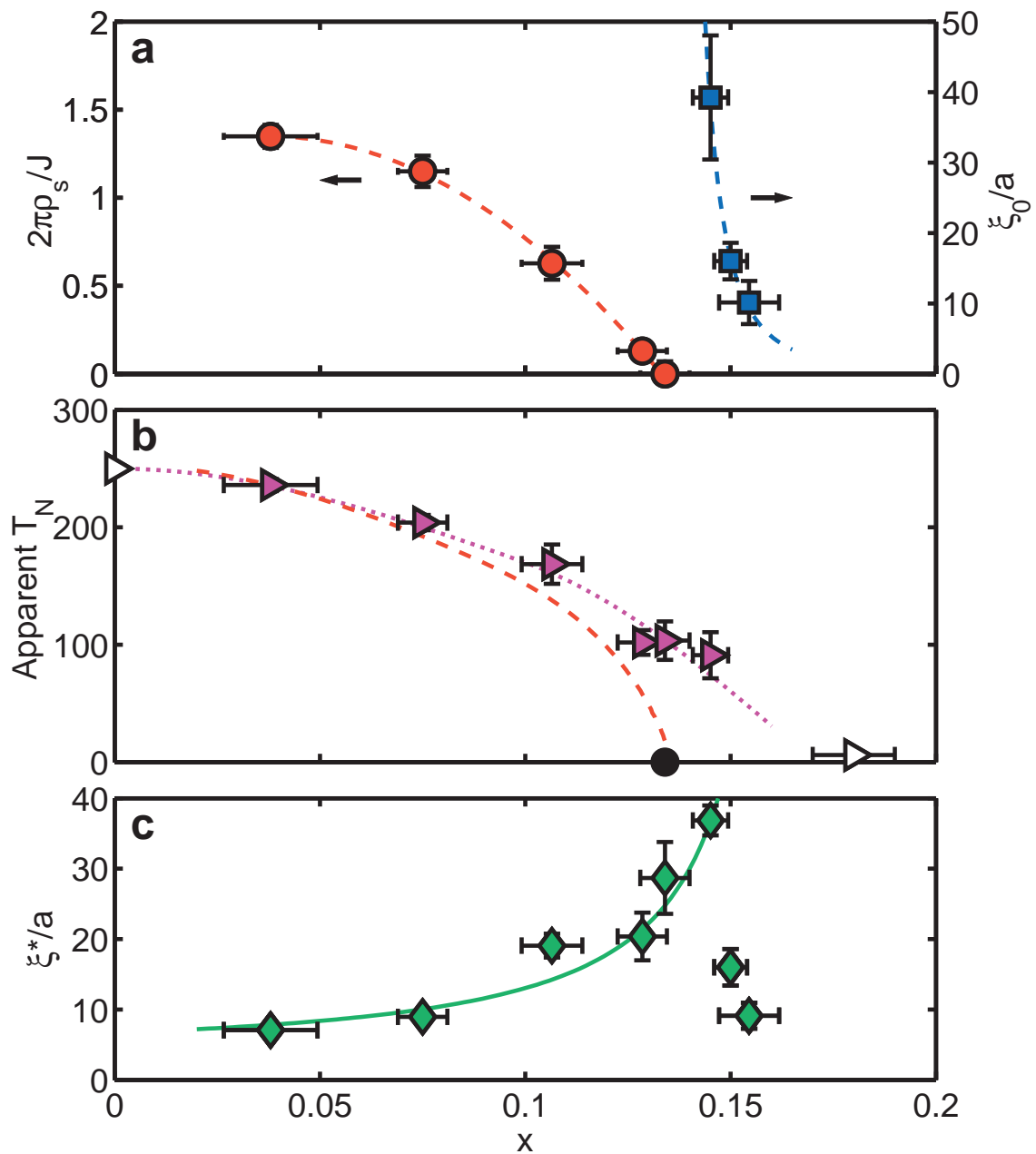


Figure 4